Energy Storage Materials 6 (2017) 26–35

Contents lists available at ScienceDirect

Energy Storage Materials

journal homepage: www.elsevier.com/locate/ensm

Lifetime *vs.* rate capability: Understanding the role of FEC and VC in high-energy Li-ion batteries with nano-silicon anodes

Tony Jaumann[a], Juan Balach[a], Ulrike Langklotz[b], Viktar Sauchuk[c], Marco Fritsch[c], Alexander Michaelis[b,c], Valerij Teltevskij[a], Daria Mikhailova[a], Steffen Oswald[a], Markus Klose[a,b], Guenter Stephani[d], Ralf Hauser[d], Jürgen Eckert[a,b,1], Lars Giebeler[a,b,*]

[a] *Leibniz Institute for Solid State and Materials Research (IFW) Dresden e.V. Institute for Complex Materials, Helmholtzstraße 20, D-01069, Dresden, Germany*
[b] *Technische Universität Dresden, Institut für Werkstoffwissenschaft, Helmholtzstraße 7, D-01069 Dresden, Germany*
[c] *Fraunhofer Institute for Ceramic Materials and Systems (IKTS) Winterbergstraße 28, D-01277 Dresden, Germany*
[d] *Fraunhofer Institute for Manufacturing Technology and Advanced Materials (IFAM), Branch Lab Dresden, Winterbergstraße 28, D-01277 Dresden, Germany*

ARTICLE INFO

Keywords:
FEC
VC
Silicon anode
Li-ion battery

ABSTRACT

Fluoroethylene carbonate (FEC) and vinylene carbonate (VC) are the most frequently used electrolyte components to enhance the lifetime of anode materials in Li-ion batteries, but for silicon it is still ambiguous when FEC or VC is more beneficial. Herein, a nanostructured silicon/carbon anode derived from low-cost $HSiCl_3$ is tailored by the rational choice of the electrolyte component, to obtain an anode material outperforming current complex silicon structures. We demonstrate highly reversible areal capacities of up to 5 mA h/cm^2 at 4.4 mg/cm^2 mass loading, a specific capacity of 1280 mA h/$g_{Electrode}$, a capacity retention of 81% after 500 deep-discharge cycles *versus* lithium metal and successful full-cell tests with high-voltage cathodes meeting the requirements for real application. Electrochemical impedance spectroscopy and post-mortem investigation provide new insights in tailoring the interfacial properties of silicon-based anodes for high performance anode materials based on an alloying mechanism with large volume changes. The role of fluorine in the FEC-derived interfacial layer is discussed in comparison with the VC-derived layer and possible degradation mechanisms are proposed. We believe that this study gives a valuable understanding and provides new strategies on the facile use of additives for highly reversible silicon anodes in Li-ion batteries.

1. Introduction

Silicon has gained tremendous attention in the last two decades as potential anode material for Li-ion batteries (LIBs) due to its high specific capacity of up to 3600 mA h/g. The development of silicon anodes is currently reaching a point for real application in commercial Li–ion batteries as advanced anode beyond commonly used graphite [1–3]. A large variety of well-designed nanostructured, thin film and amorphous silicon anodes have been proven to overcome the general issue of a low reversibility [4–9]. The high production costs and unsatisfactory lifetime are two major issues preventing its broad commercialization. Among others, one of the most promising strategies to overcome the low reversibility is the use of modified electrolytes or electrolyte additives. These additives, if well designed, have the ability to form a stable solid-electrolyte-Interface (SEI), a typical surface film on any anode material in LIB composed of reduced electrolyte components [10]. Its stability is essential for long lifetime and safe operation of LIB owing to the prevention of continuous electrolyte decomposition. The SEI on silicon is challenging to stabilize due to the large volume changes during lithium insertion which is the main critical reason for high degradation [11]. It was shown that particular compounds have the ability to form a flexible SEI on silicon surviving the volume changes and to open the way for application of even low-cost silicon anodes with excellent cycling stability [12–15]. Fluoroethylene carbonate (FEC) is one of the best-known and most studied additives for silicon anodes in Li-ion batteries [15] and is

* Corresponding author at: Leibniz Institute for Solid State and Materials Research (IFW) Dresden e.V. Institute for Complex Materials, Helmholtzstraße 20, D-01069 Dresden, Germany.
E-mail address: l.giebeler@ifw-dresden.de (L. Giebeler).
[1] Present address: Austrian Academy of Sciences, Erich Schmid Institute of Materials Science, Jahnstraße 12, A-8700 Leoben, Austria and Montanuniversität Leoben, Department Materials Physics, Jahnstraße 12, A-8700 Leoben, Austria.

http://dx.doi.org/10.1016/j.ensm.2016.08.002
Received 25 May 2016; Received in revised form 12 August 2016; Accepted 31 August 2016
Available online 21 September 2016

nowadays a standard additive for testing silicon anodes [9,16–22] because of its significant positive effect on the reversibility [13,15]. Vinylene carbonate (VC), already commercialized for LIB in order to increase the Coulombic efficiency and thermal stability of graphite, is another well-known additive with longer history in battery application than FEC [23]. VC is considered to be the most effective additive for enhanced lifetime of graphite anodes [10,24] and is sometimes used for silicon anodes as well [1,11,25]. FEC and VC were both reported nearly at the same time for silicon to enhance the stability of thin film silicon anodes [15,26], but FEC became the most frequently used additive for silicon anodes [27] although the superior properties of FEC for silicon have not clearly been proven yet and literature shows partially contrary results. Dalavi *et al.* and Leveau *et al.* evaluated both additives on thin film as well as nanostructured silicon anodes and found very similar results [28,29]. In contrast, Uchida *et al.* found enhanced performance with FEC on micro-structured silicon [30]. The reason for such partially controversial results maybe found in different anode design and in similar chemical structures as well as decomposition products of both additives. It is well accepted that both additives form a flexible and stable layer on the surface which can accommodate the large volume changes of silicon during lithiation. Their chemical structure is closely related to ethylene carbonate and similar final polymeric products were proposed [31] and postulated by DFT calculation [32]. The polymeric products were proven to be polycarbonates for VC and it is well-accepted that they are the origin for enhanced reversibility [26,33,34]. In the case of FEC, the origin of an enhanced reversibility is still discussed controversially. It has been consistently reported that FEC causes increased LiF formation, but the role of LiF on silicon is not clear. Etacheri *et al.* found polycarbonates as decomposition product of FEC [31] suggesting that LiF may not be responsible for an enhanced reversibility but rather VC-derived products, which agrees well with our previous study [35]. Other studies report on fluorinated polymers [36,37] or stable LiF-rich layered SEIs, which are formed as essential compounds for high reversibility [15,38,39]. From experiences of commercial electrolyte systems and anode materials (*i.e.* graphite) in LIBs, the formation of LiF seems not to stabilize the reversibility [10,40]. In this regard, we recently reported that massive LiF formation cannot stabilize the reversibility of nanostructured silicon anodes in ether-based systems [41]. In order to identify the role of fluorine, a comparative study between VC and FEC seems to be the most promising approach to shed light on this matter. It must be noted that the choice of VC or FEC as additive in LIB not only depends on the positive effect on the anode, but also on the cathode. Shin *et al.* reported that FEC seems to have a detrimental effect to the cathode (LMO) side especially at elevated temperature because of increased HF release [42], whereas some other groups reported positive effects on high-voltage cathodes with FEC [43,44]. Burns *et al.* studied 18650 cells with graphite/NCM materials and found the lowest cycle lives for FEC [45]. VC offers higher thermal stability [46] and is mainly considered to have a positive influence on the cathode performance [33]. In order to enhance the lifetime of LIBs equipped with advanced silicon-based anodes, a fundamental discussion with respect to these additives is required. In this contribution, we provide new insights into the anodic mechanism of both additives and unveil advantages and disadvantages of FEC and VC additives for high-capacitive nanostructured silicon anodes with excellent lifetime.

For this purpose, both electrolyte additives were evaluated in a commercial electrolyte on a high-capacitive and low-cost nanostructured silicon/carbon anode comprised of small-sized silicon nanoparticles attached to a porous carbon scaffold. The electrochemical performance of our nanostructured material is governed by its surface characteristics defined by the small size of the silicon nanoparticles (smaller than 5 nm) and the high surface area. It allows a detailed analysis of degradation phenomena caused by an instable SEI. Other degradation phenomena, especially material pulverization, can be neglected, since the crystallite size is determined far to be lower than the critical crack lengths of silicon [47]. We will first characterize the nanostructured silicon/carbon anode and proceed with the electrochemical testing. Post mortem investigations of cycled electrodes will be reported followed by a fundamental discussion to understand the degradation phenomena by the SEI. Finally, we demonstrate a highly reversible nanostructured silicon-based anode capable to deliver a high specific capacity of 1280 mA h/$g_{Electrode}$ and an areal capacity of up to 5 mA h/cm^2 outperforming current complexly designed silicon anodes. The superior performance was verified in real systems by testing the silicon anode versus high-voltage cathode materials.

2. Experimental section

2.1. Synthesis of nanostructured silicon/carbon (Si@C)

We used a modified synthesis of our previous report which offers higher capacities, but therefore poorer reversibility [9,35]. In a typical synthesis, 10 ml of $HSiCl_3$ (Sigma-Aldrich, > 99 vol%) were provided in a three-neck round-bottom flask cooled with an ice bath (~−5 °C), flushed and kept under argon using standard Schlenk technique in order to allow a safe polycondensation [48]. Under vigorous magnetic stirring, 0.2 ml ethanol (> 99.9 vol%) were slowly injected through a septum and 10 min later 8 ml of deionized water were slowly added. One exhaust of the flask was connected with a hose leading to a beaker filled with 0.1 M NaOH in order to neutralize the generated HCl. After the injection of water, the flask was kept for 1 h in the ice bath to complete the reaction. The flask was heated to 80 °C for 3 h under argon flow in order to remove unreacted $HSiCl_3$ and HCl. Finally, the obtained white powder was dried under dynamic vacuum over night and was then ground in a mortar. The $(HSiO_{1.5})_n$ precursor was annealed with an infrared oven (Gero LHTG 150-200/30-1G) at 1150 °C ± 20 °C in argon atmosphere for 2 h at a heating rate of 50 °C/min up to 800 °C and 12.5 °C/min up to 1150 °C. Afterwards, the composite was again ground. 150 mg sucrose and 1.5 g of the annealed material were mixed together in 5 ml of 3 wt% H_2SO_4 and sonicated for 1 h at 50 °C before heating to 100 °C under vigorous stirring for another 1 h. The black powder was dried at 150 °C for about 4 h. The sucrose coating procedure was repeated once. Finally, the material was annealed at 900 °C (5 °C/min heating rate) for 5 h under argon flow to carbonize the sucrose. About 1.5 g of the carbonized material was mixed with 15 ml deionized water and 3 ml HCl in a Teflon beaker equipped with a magnetic stirring bar. Under vigorous stirring 7.5 ml of HF (40 wt%) was slowly added and the suspension was stirred for no longer than 25 min in total to selectively remove the silicon oxides. The solution was filtered and washed twice with deionized water and once with ethanol within 30 min. Finally, the product was dried under vacuum overnight and stored under argon. Long exposure (more than 5 h) to air should be avoided due to the unknown stability of the silicon nanoparticles.

2.2. Material characterization

X-ray powder diffraction (XRD) was performed with a STOE Stadi P diffractometer with curved Ge(111) crystal monochromator and 6°-position sensitive detector. The as-synthesized powder was fixed between acetate foils with a collodion glue. The samples were measured in the range of $10° \leq 2\theta \leq 90°$ with a step size of $\Delta 2\theta = 0.01°$ in transmission geometry with Cu $K_{\alpha 1}$ radiation. Rietveld-analysis was performed with the program MAUD [49] and the Popa-line broadening model assuming isotropic crystallite size. Scanning electron microscopy (SEM) was carried out with a LEO Gemini 1530 microscope. The acceleration voltage was 10 kV and a Bruker detector (XFlash 6) was used for energy dispersive X-ray (EDXS) analysis. For transmission electron microscopy (TEM) a FEI Tecnai F30 with field emission gun and 300 kV acceleration voltage was applied. Thermo gravimetric analysis in synthetic air was conducted with a Netzsch Jupiter STA

449C. X-ray photoemission spectroscopy (XPS) has been conducted by a Physical Electronics PHI 5600 CI system with Mg Kα (1253.6 eV) radiation (350 W) at a pass energy of 29 eV and a step size of 0.1 eV. Standard single-element sensitivity factors were used to calculate the elemental concentrations from the XP spectra. The core level signals were fitted with a Gaussian function (MagicPlot Software) using a basic linear background after normalization to 1. For post-mortem investigation, the cells were cycled 300 times at I=500 mA/g between 0.01–1.2 V *vs*. Li/Li$^+$ and disassembled in the delithiated state inside a glove box under argon atmosphere ($H_2O < 1$ ppm, $O_2 < 0.1$ ppm). Each electrode was washed three times in 1 ml DMC. For XRD analysis, the samples were pressed between Kapton tapes under argon atmosphere to avoid contact with air during scanning. For the sample transfer into the SEM, the samples was exposed to air for about 1 min.

2.3. Electrochemical testing

A slurry of Si@C (85%), Super P Li (Timcal) (10%) and polyacrylic acid (Sigma-Aldrich, M_v ~ 450 000) (5%) was prepared in ethanol under ambient conditions by a ball milling for 15 min. Ethanol-based slurries turned out to be the optimal solvent for electrode fabrication in air of this material. The homogeneous slurry was blade casted (250 µm wet thickness) on copper foil (MTI Corp., 10 µm thickness). After 20 min. of drying, 12 mm electrodes were punched out and transferred to the glove box to avoid further oxidation of the active silicon species. The mass loading on each electrode was determined by a micro balance (Mettler Toledo XSE) and accounts to 0.7 mg/cm^2. Because of serious issues in structural integrity of high mass loadings, a cellular copper mesh structure infiltrated with the slurry was used to obtain mass loadings of up to 5 mg/cm^2. The preparation and the characteristics of the 3D copper structure is placed in the supporting information. (Fig. S1 and Fig. S2) All electrodes were dried at 100 °C over night under vacuum prior to assembly in Swagelok cells under argon atmosphere ($H_2O < 1$ ppm, $O_2 < 0.1$ ppm). Two glass fiber layers (Whatman) were used as separator and lithium metal (250 µm thickness, Chemetall) as counter electrode. The reference electrolyte was 1 M $LiPF_6$ in EC/DMC (1:1) (LP30 Selectilyte, BASF) and 10 vol% vinylene carbonate (Sigma-Aldrich, > 99.9%) or 20 vol% fluoroethylene carbonate (Sigma-Aldrich, > 99.9%) were used as additive, if not otherwise mentioned. A BaSyTec Cell Test System was used for galvanostatic cycling in the range of 0.01–1.2 V *vs* Li/Li$^+$ (half-cell). The current rates were based on the mass of Si@C and the capacities were calculated on the entire electrode mass (without copper). For full-cell tests, tape cast high-energy NCM (HE-NCM) electrodes were used as cathode. Details on the synthesis of the active material and on the electrode preparation are given in the support information. Full-cells (Si vs HE-NCM) were cycled between 1.8–4.6 V. Prior to full-cell assembling, the silicon anodes were pre-cycled twice between 0.01–1.2 V *vs*. Li/Li$^+$ at 250 mA/g and disassembled at 0.4 V in order to compensate lithium loss due to initial SEI formation. The silicon anode was roughly 40–

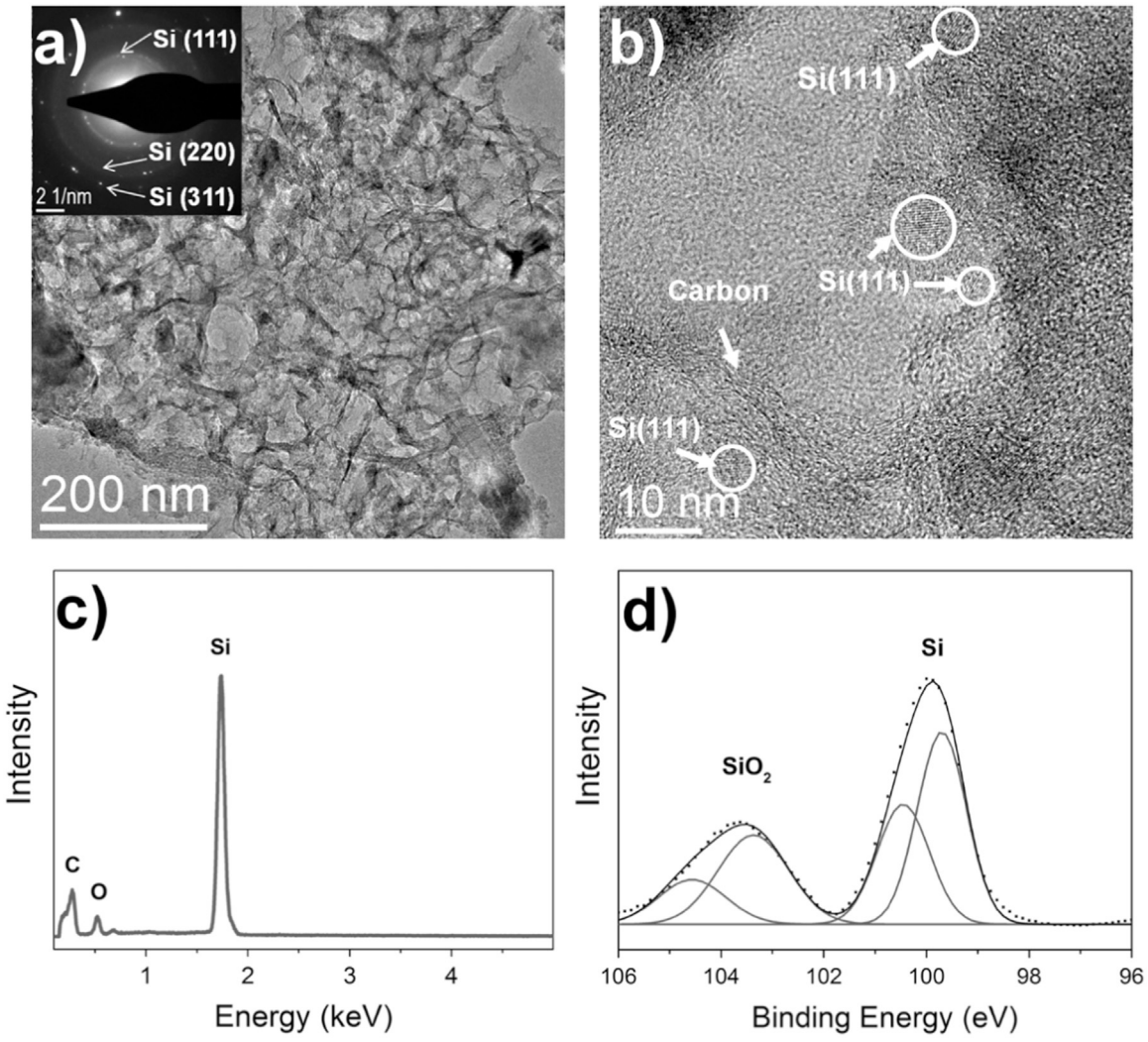

Fig. 1. a) TEM bright-field image of the silicon/carbon composite with the corresponding SAED pattern (inset), b) High-resolution image, c) EDX spectrum of the Si@C and d) XP spectrum of the Si 2p core level of the prepared electrode.

80% over dimensioned in terms of capacity. For electrochemical impedance spectroscopy (EIS) a VMP3 system (Biologic) was used. The amplitude was 5 mV and the frequency range was 1 MHz–10 mHz. The spectrum was taken in the delithiated state at 1 V *vs.* Li/Li^+. The fits of the equivalent circuit were carried out with the EC-lab software. All measurements were recorded at 25 °C in a climate chamber.

3. Results

3.1. Morphology of the nanostructured silicon/carbon (Si@C)

The synthesis of the Si@C requires a condensation of low-cost trichlorosilane with water to form the hydrogen silsesquioxane (HSQ), a temperature treatment and an etching procedure, making it an attractive candidate for up-scaling processes. Note that HSQ is also commercially available. The structure of the silicon/carbon nanocomposite was characterized by electron microscopy and X-ray diffraction. TEM bright-field images (Fig. 1a) show agglomerated hollow carbon spheres with diameters of 50–150 nm, which are partially open probably because of incomplete carbon coating with sucrose and the etching procedure. As can be seen from high-resolution TEM images (Fig. 1b), silicon nanoparticles depicted by the crystalline (111) lattice planes are attached at the outside and inside of these carbon spheres. We also observe some bigger silicon crystallites of up to 100 nm depicted by the dark areas in the TEM image (Fig. 1a) and concluded from the SAED pattern (Fig. 1a, inset) as point reflections typical for oriented large crystallites. EDXS analysis with a scanning electron microscope proves the presence of silicon and carbon (Fig. 1c). The as-prepared Si@C electrode was studied by XPS in order to characterize the surface species and the stability of silicon nanoparticles. The XP spectrum of the Si 2p core level (Fig. 1d) clearly proves the presence of predominantly elemental silicon (63 at%) along with some silica (SiO_2, 37 at%) due to surface oxidation and incomplete etching. Each species is represented by two functions due to spin-orbit coupling. Note that silica is present on any silicon surface as native oxide layer. The results further demonstrate that the material can be fabricated to electrodes under ambient conditions without significant oxidation.

XRD was performed for both, the temperature treated HSQ precursor and the final Si@C. In both cases, the XRD pattern (Fig. 2a) show broad reflections corresponding to the cubic silicon structure ($Fd\bar{3}m$) with a lattice constant of 5.431 Å indexed by the Bragg positions (green). The broad reflection at 21° mainly corresponds to silica, but may also result from the background (polyacetat foil and collodium glue). As expected the peak intensity of the silicon phase and the Si/SiO_2 ratio in the Si@C increases because SiO_2 is etched during preparation, while the silicon remains within in composite. The results demonstrate the successful formation of silicon nanoparticles and their retained structure after the etching process to remove the silica. The crystallite size of silicon was determined to be 3 nm, which corresponds well to our recent studies [9]. We also determined some large crystallites of 50–70 nm. The Bragg positions of both phases merely change due to similar lattice constants, thus presented only once for the small silicon crystals as main phase. The mass of the larger crystals is rather low and accounts to roughly 5 wt% considering the crystalline silicon phases, which have been observed by TEM investigations as well. These crystallites may result from the rapid heating during annealing in the oven in order to prevent diffusion of SiH_4 [48,50]. The total silicon content in the carbon composite was determined by thermogravimetric (TGA) combustion in air (Fig. 2b).

Initially, the mass curve increases along with temperature due to oxidation of silicon nanoparticles and drops at about 500 °C because of gaseous CO/CO_2 formation. Since both oxidation processes occur simultaneously, the carbon loss at about 500 °C is little accurate to determine the ratio of Si/C within the composite. Therefore, we took the final mass at the end of combustion to determine a silicon content of about 53 wt% assuming that only SiO_2 remains after combustion at

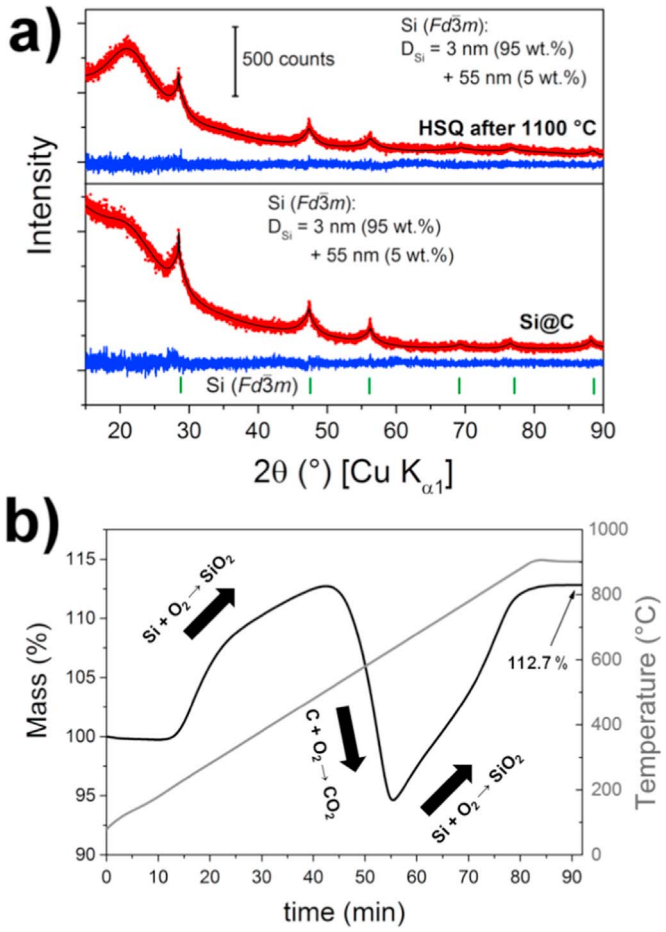

Fig. 2. a) observed XRD (red) and calculated (black) pattern with difference line (blue) of the Rietveld analysis with crystallite sizes and phase contents of the temperature treated HSQ precursor and after processing to Si@C, b) TGA combustion of Si@C in synthetic air at a heating rate of 10 °C/min to 900 °C.

900 °C [51]. From the overall results, the structure of the material at hand is best described as a porous carbon scaffold with attached silicon nanoparticles of sizes below 5 nm. Note that the small particle size below 5 nm with high surface area is not only beneficial for the analysis of the surficial SEI formation through different electrolyte additives, but also positive for enhanced reversibility compared to conventional silicon nanoparticles [52].

3.2. Electrochemical performance (half-cell)

The electrochemical performance was studied by galvanostatic cycling between 0.01–1.2 V *vs.* Li/Li^+ at current rates of 250 mA/g to 4 A/g in a commercial electrolyte 1 M $LiPF_6$ in EC/DMC (1:1) for LIB in dependence of FEC and VC addition.

Initially, the electrochemical performance was analyzed in dependence of the FEC concentration in the electrolyte and the current rate. Commonly, the concentrations of additives in commercial LIB are 1–2 vol% [24]. However, in contrast to graphite anodes, the large volume changes and high surface area of nanostructured anodes consume considerable more electrolyte to form a stable SEI. Thus a remarkably higher amount of additives up to 20 vol% is necessary to maintain a good performance. We added 10 vol% and 20 vol% of FEC to the electrolyte, which is according to literature the range that offers best performance for silicon anodes [13,35,37,44]. For comparison, the VC concentration was set to 10 vol%, which was reported to show highest reversibility on graphite anodes and LIB full cells [24]. The addition of high amounts of FEC/VC does not substantially influence the ion

Table 1
The resistances determined by EIS in dependency of electrolyte additive and cycle number. Values were calculated with the equivalent circuit model in Fig. 4a.

Electrolyte	Cycle number	R_{El} (Ohm)	$R_{SEI+Int}$ (Ohm)	R_{CT} (Ohm)
w/o	1	10	47	2
	300	16	115	1154
20 vol% FEC	1	10	28	5
	300	14	36	546
10 vol% FEC	1	12	18	2
10 vol% VC	1	10	47	8
	300	10	80	75

conductivity of the electrolyte as concluded from impedance spectroscopy (Table 1). The results of galvanostatic cycling are shown in Fig. 3a. The first delithiation capacity of around 1280 mA h/$g_{Electrode}$ is independent of the electrolyte composition and almost 4 times higher than for graphite-based anodes in commercial Li-ion batteries. Note that the capacity is based on the total weight of the electrode. The capacity based on the mass of silicon is calculated to 3000 mA h/$g_{Silicon}$ initially, which is about 85% of the theoretical value for silicon (≈3600 mA h/g) [6]. The capacity resulting from the carbon can be neglected [41]. Lowest reversibility is observed without any additive, as expected. The specific capacity rapidly drops to 244 mA h/$g_{Electrode}$ and 20% of its initial value, respectively, after 100 cycles independent of the current rate. FEC addition enhances the reversibility. In this case the capacity still reaches 63 % of the initial value and 796 mA h/$g_{Electrode}$, respectively, after 100 cycles at 250 mA/g. At a higher current rate of 500 mA/g the capacity and reversibility is merely affected. Importantly, the reversibility is independent of the FEC concentration in the range of 10 vol% and 20 vol%. For both FEC concentrations a capacity loss of 30–40% after 100 cycles is observed independent of the current rate. With VC addition the reversibility is even more improved and outperforms both concentrations of FEC in the electrolyte. After 100 cycles a capacity of 1045 mA h/$g_{Electrode}$ is observed, which corresponds to 80% of the initial value. Considering the fact that the capacity drops to 1080 mA h/$g_{Electrode}$ already in the initial seven cycles, the capacity fading in the following 100 cycles accounts to only 3%. Such a dramatic effect of VC has not yet been reported for any type of silicon anodes [24]. However, in contrast to the additive-free and FEC containing electrolyte, high current rates drastically reduce the capacity in the case of VC addition. While at 250 mA/g the capacity is comparable to the FEC-containing electrolyte, the capacity significantly drops at a twofold current rate.

From the results, we conclude that i) the concentration of FEC between 10 and 20 vol% in the electrolyte merely affects the reversibility of our silicon anode and ii) the 10 vol% VC addition to the electrolyte clearly outperforms both low and high FEC concentrations in the electrolyte. However, at high current rates, the capacity with VC significantly drops, indicating high resistance.

The Coulombic efficiency (CE) provides further information about side reactions on the surface of the electrode (Fig. 3b). Initially, a high amount of electrolyte is consumed to form a protective SEI on the composite. The electrolyte consumption is highest with VC since the CE is only 53% and increases to 55% with FEC addition at the same volume concentration. The highest CE is obtained without any additive as found in our previous report [35]. After the first two cycles, the CE is highest with VC and reaches more than 99% after the 20th cycle. Also with FEC addition the CE is considerably higher than without any additive suggesting less side reactions during cycling, but still lower compared to VC. Without any additive the CE is always lower than 97% indicating high electrolyte consumption during the cycling period. The discharging/charging curves of the first cycle are presented in Fig. 3c. The prompt decomposition of FEC is clearly visible as plateau at a potential of around 1.47 V *vs.* Li/Li^+ independent of the FEC concentration. In contrast, VC decomposition shows a different behavior and

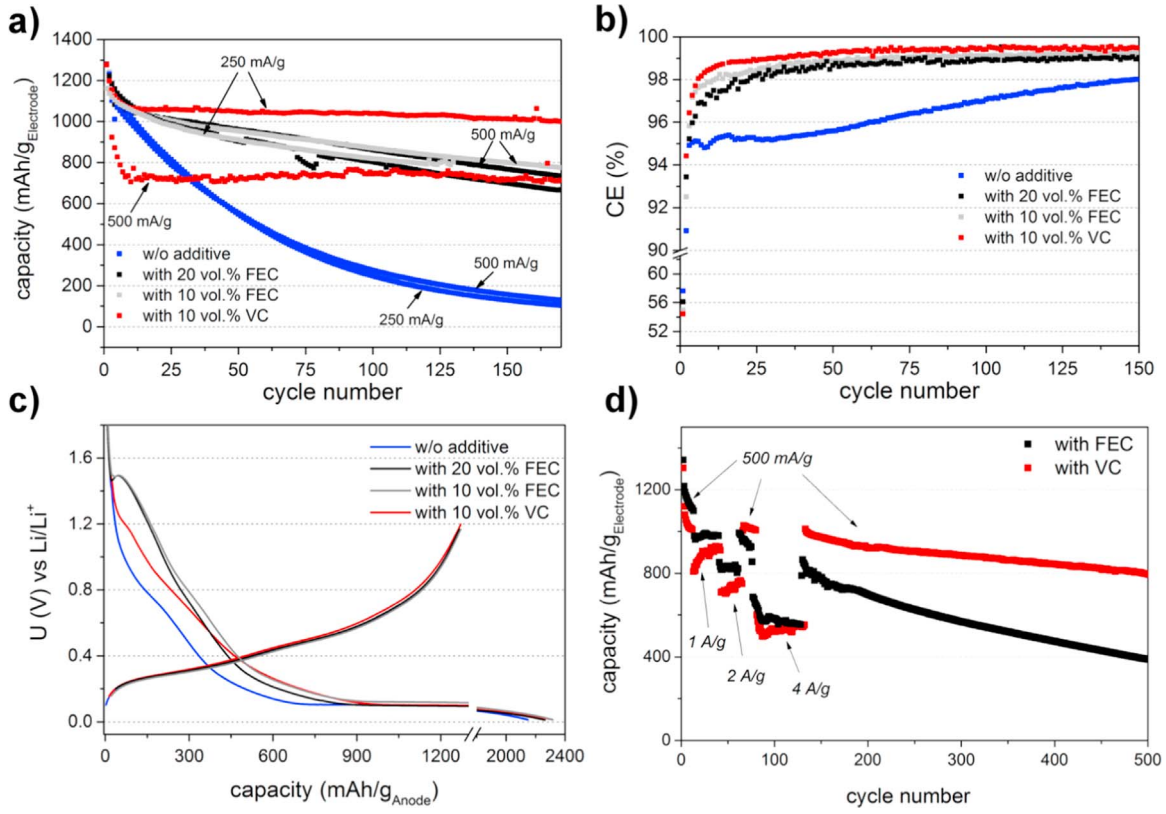

Fig. 3. Galvanostatic cycling of the Si@C electrode between 0.01–1.2 V *vs.* Li/Li^+ in dependence of VC and FEC addition a) at 250 mA/g and 500 mA/g, b) the corresponding Coulombic Efficiency (CE) at 250 mA/g, c) the discharging/charging curves of the first cycle and d) long-term cycling at 250 mA/g–4 A/g with 20 vol% FEC or 10 vol% VC.

is depicted as a gradual slope starting at around 1.25 V *vs.* Li/Li^+ similar to the EC/DMC decomposition at ≈0.8 V *vs.* Li/Li^+ in the additive-free electrolyte.

Further long-term experiments at different current rates ranging from 0.25 A/g to 4 A/g were carried out in dependence of FEC and VC addition (Fig. 3d). Best rate capability is achieved with FEC addition whereas the capacity with VC considerably drops to lower values with increasing current rates and shows about 15% lower capacity at 2 A/g compared to FEC. However, the faster degradation with FEC compared to VC is clearly visible and after 125 cycles the VC electrolyte outperforms the FEC electrolyte even at high current rates of 0.5 A/g because literally no degradation occurs with VC. After 500 cycles in VC only 19% capacity loss is observed neglecting the initial capacity drop after the first 7 cycles. In contrast, the reversibility in the FEC electrolyte is relatively poor and the degradation accounts to 65% after 500 cycles. These results confirm our preliminary tests and clearly suggest that VC outperforms FEC in terms of reversibility likely because of an extremely stable SEI.

The results agree well with Leveau *et al.* and Dalavi *et al.* They observed slightly enhanced performances with VC on silicon nanowires and amorphous silicon thin films, respectively, independent of different concentrations of FEC and VC [28,29]. In contrast, Uchida *et al.* observed enhanced reversibility with FEC [30], which may be attributed to the use of micro-sized silicon particles suffering from crack propagation of individual particles during volume changes as an additional degradation mechanism [47]. However, VC seems to cause a high impedance and considerable internal resistance (IR-drop) since the rate capability is poor. The reason may be found in different charge and mass transport conductivity on the electrode surface influencing the rate capability. In order to study these transport processes and to corroborate our findings, we performed electrochemical impedance spectroscopy (EIS) at different cycling states (for I=500 mA/g) and post-mortem investigations. EIS is a powerful technique to evaluate mass and charge transport processes in the battery. By applying different frequencies at defined AC potentials, the response of various resistances resulting from mass transport inside different phases and charge transfer processes at the phase boundaries can be separated and measured. The electrolyte and other Ohmic resistances are typically determined at high frequencies of around 1 MHz–100 kHz and may be modeled as a simple resistor element R. The film resistance for Li^+ migration through the SEI (R_{SEI}) coupled with film capacitance and the impedance of the substrate/electrode interface (R_{Int}) are evaluated in the frequency range of around 1 kHz–10 Hz and is typically modeled as a parallel constant phase element and resistor circuit $Q \parallel R_{SEI+Int}$. The charge transfer resistance (R_{CT}) at the phase boundaries typically observed at frequencies of 10 Hz–0.1 Hz is also modeled as a $Q \parallel R_{CT}$ circuit. Charge transfer corresponds to Li^+ transfer at the film/silicon interface and interparticle electron transfer from silicon to carbon [53]. At frequencies below somewhat 40–20 mHz the transport processes of solid state diffusion are evaluated, herein modeled as series of a Warburg element (W) and a capacitor (C) [53–55]. The impedance contribution of the counter electrode, here metallic lithium, will be neglected because of the low surface area and presumably equal contribution in all electrolyte compositions [56]. Fig. 4b shows the Nyquist plots in dependence of electrolyte additive and cycle number. Additionally, the Bode plot is provided in the support information (Fig. S3) to evidence the dependence of the impedance on the frequency. The electrolyte resistance at high frequencies is constant and independent of the additive addition. After the first cycle all impedance spectra show a semi-circle at frequencies of 10 kHz–10 Hz, majorly corresponding to the film resistance of the SEI. By applying the equivalent circuit model (Fig. 4a), we find the lowest film resistance of 28 Ω for FEC addition (Table 1). With VC and without any additive the film resistance is considerably higher and accounts to 47 Ω. This result is consistent with other reports. For example, Burns *et al.* observed increasing impedance with higher concentrations of VC at a prolonged cell life on graphite anodes [24]. Uchida *et al.* also reported higher impedance with VC on micro-sized silicon anodes [30]. These results well confirm the observations described here and suggest a very similar SEI structure and probably SEI formation on silicon and graphite. The R_{CT} determined for all electrolyte configurations is rather low after the first cycle (2–8 Ω), since the SEI is still relatively thin and interparticle electron transfer may not be hindered. After long-term cycling the impedance increased dramatically without additive and reaches overall the highest values with a $R_{SEI+Int}$ of 115 Ω and a R_{CT} of 1154 Ω.

These results suggest a rapidly growing SEI which is neither ionically nor electrically conducting. Probably, the thick surface film isolates the active silicon particles from the conductive carbon causing low reversibility. With FEC as electrolyte additive the overall impedance is significantly lower after long-term cycling. $R_{SEI+Int}$ remains almost constant and reaches up to 36 Ω. However, R_{CT} increases dramatically to about 546 Ω. This result indicates an unstable SEI, non-resistant to withstand the dramatic volume changes, causing a continuously growing SEI. Although the instable SEI remains well conductive for ions, R_{CT} increases dramatically, which is attributed to the electron transfer between silicon and carbon. Hence, the electronic

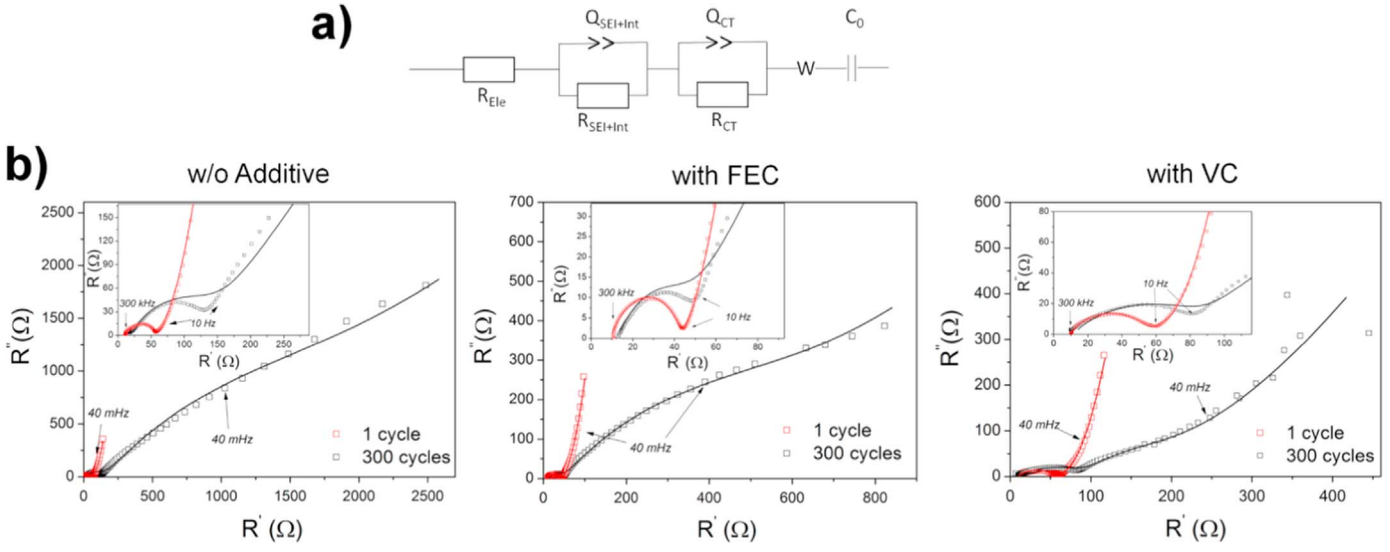

Fig. 4. a) Equivalent circuit model for determination of resistance values R with W= Warburg element, C= capacitor, Q= constant phase element and b) Nyquist plots after 1 cycle and 300 cycles in dependency of the electrolyte composition. The mass loading was 0.9 mg ± 0.4 mg per electrode.

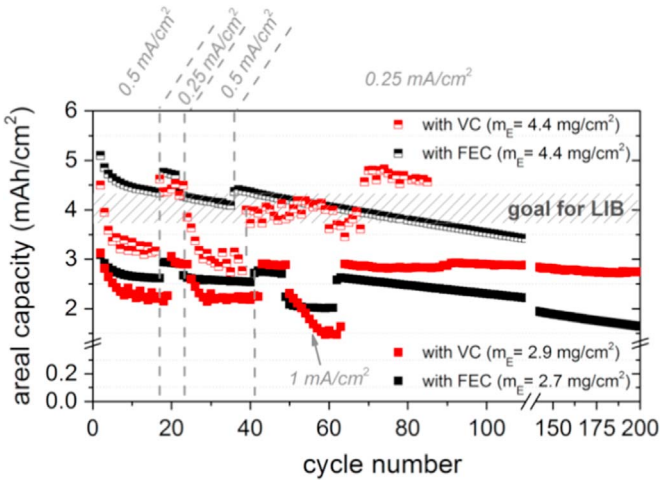

Fig. 5. Areal capacity of Si@C with different electrode masses (m_E). The electrodes were galvanostatically cycled *vs.* Li/Li^+ between 0.01–1.2 V in dependency of FEC or VC addition at current density of 0.25 mA/cm², 0.5 mA/cm² and 1 mA/cm².

contact of the active species slowly decays and is eventually lost, causing a continuous degradation even for FEC addition. In contrast, for VC the overall impedance is lowest after long-term cycling. The $R_{SEI+Int}$ after 300 cycles increases from 47 Ω to 80 Ω, while the R_{CT} only increases to 75 Ω, which is remarkably low compared to the other electrolyte compositions. VC seems to form a very stable surface film, which merely changes its transport and charge transfer process characteristics over cycling. VC therewith exhibits a clearly different behavior and has a much higher impact on cycle life and lifetime of a cell compared to the FEC-containing and the additive-free electrolyte.

In order to demonstrate the practical relevance of our findings, we tested the nanostructured composite with high mass loading in both additives, FEC and VC. The results are shown in Fig. 5.

With FEC addition high areal capacities of 3 to 5 mAh/cm² at mass loading of 2.8–4.4 mg/cm² are obtained at current rates of 0.5 mA/cm² and even at high current rates of 1 mA/cm² the capacity merely drops. However, the degradation for the FEC electrolyte is clearly visible and after 100 cycles about 22% of the initial capacity is lost. With VC as electrolyte additive the initial areal capacity is comparable to the FEC electrolyte at low current rates of 0.25 mA/cm² and at mass loadings of 3 mg/cm², but higher current rates of 0.5 or even 1 mA/cm² cause a drastic drop of the capacity. Additionally, a high mass loading of up to 4 mg/cm² reduces the capacity of the cell with the VC electrolyte compared to FEC due to the increasing impedance. However, the reversibility is still excellent and almost no degradation is observed even after 170 cycles. We compared our results to current complex silicon/carbon nanostructures tested as anode in LIB (Table 2).

Liu *et al.* prepared complex hollow nano-silicon/carbon electrodes and demonstrated 100 cycles at 3 mA h/cm² with 3.12 mg/cm² mass loading [1]. The capacity loss after 100 cycles was almost zero. Peled *et al.* tested silicon nanowires on gas-diffusion-layers (GDL) with 2–5 mA h/cm² and reported 16–35% capacity loss after 200 cycles [19]. Both studies used VC and/or FEC. Comparable results are obtained by using a simple nano-silicon/carbon anode. We highlight reversible areal capacities of 4–5 mA h/cm² at a low mass loading of 4.4 mg/cm² meeting the requirements for real application in LIBs achieved by a low-cost silicon/carbon nanocomposite.

Table 2
Comparison to some outperforming nano-silicon/carbon anodes recently reported in literature. Galvanostatic cycling: 0.01–1.0 V *vs.* Li/Li^+.

Reference	Initial capacity (mA h/cm²)	Mass loading (mg/cm²)	Current (mA/cm²)	Cycle number	Capacity loss after cycle number (%)*
[1]	3.1	3.1	0.7	100	0–3
[19]	2–5	1.0–1.5 (+3.8$_{GDL}$)	0.1	200	16–38
Here	3–4.5	2.9–4.4	0.25	80–170	0–3

* The first cycle was not considered in the calculation

3.3. Electrochemical performance (full-cell)

As already pointed out, the choice of the additive not only depends on the anode, but also on the cathode material. Therefore, we tested our silicon anode *versus* HE-NMC cathodes of the composition $Li_{1,23}Mn_{0,61}Ni_{0,15}Co_{0,005}O_2$ in order to prove that our findings are adaptive to real full-cell systems and that high concentrations of FEC/VC can indeed be used in LIB. The HE-NCM cathode material enables electrode potentials up to 4.8 $V_{Li/Li+}$, going along with an oxidative decomposition of the electrolyte. Thus, the effect of the additives is of higher interest in this case, compared to common cathode materials such as LFP (3.6 $V_{Li/Li+}$) or even $LiCoO_2$ (up to 4.3 $V_{Li/Li+}$). Therefore, the general compatibility of the HE-NCM with FEC-containing electrolytes had been tested in half-cells before. These tests showed no negative effect of the additive concerning the capacity or the degradation behavior of the cathode. Moreover, a lower internal resistance of the cell was observed, indicating a less distinct film of decomposition products deposited onto the cathode surface. These results are in accordance with other studies [24,43]. The first charge/discharge curves of the full cells are shown in Fig. S4. They are dominated by the electrode potential course of the cathode, showing the typical plateau for HE-NMC materials independent of the chosen electrolyte [43]. The results of galvanostatic long-term cycling between 1.8–4.6 V at current densities ranging between 0.25 mA/cm² to 1 mA/cm² are depicted in Fig. 6a/b. First and most important, all electrolyte compositions are successfully employed in full-cells and show good cycle stability. In the first cycles, a capacity increase from about 80 mA h/$g_{cathode}$ to a maximum of about 110 mA h/$g_{cathode}$ is found which may be related to the activation of both the cathode and anode. Theoretically, HE-NCM can deliver up to 200 mA h/$g_{cathode}$ when higher potentials up to 4.8 V are applied. However, the limitation of the cell voltage to 4.6 V remarkably increases the cycling stability of the cathode material. As the scope for this study is to examine the behavior of the anode, a possibly disturbing effect of a prematurely aged cathode can be excluded.

With respect of the VC or FEC addition to the electrolyte, we observe the same trend as already found for half-cells. This finding suggests that the electrolyte has the most significant impact on the silicon anode. Without an additive, the cycle stability and CE is clearly least, presumably originating from an instable SEI on the silicon anode. The addition of FEC increases the long-term cycle stability (Fig. 6a) and the overall CE up to 1% (Fig. 6b). However, the electrochemical performance is marginally improved as expected based on the half-cell measurements and the capacity after 100 cycles accounts to 82 mA h/g_{HE-NCM}, only slightly higher than w/o additive (77 mA h/g_{HE-NCM}). This observation might indicate that FEC has a negative impact at certain conditions on the cathode, also suggested by Shin *et al.* [44]. Nevertheless, this behavior is contradictory to the results on HE-NMC half-cells and has to be investigated in detail. With VC in the electrolyte, the long-term cycle stability and efficiency are far highest indicating a stable SEI on the anode. After 100 cycles still 96 mA h/g_{HE-NCM} are obtained and the CE reaches 99.8% almost fulfilling the requirements for practical application. In the beginning the rate capability is slightly lower compared to the FEC-containing electrolyte composition due to higher resistance as already found for half-cells. Overall, these findings are in accordance with the half-cell tests and clearly prove the relevance for real Li-ion systems.

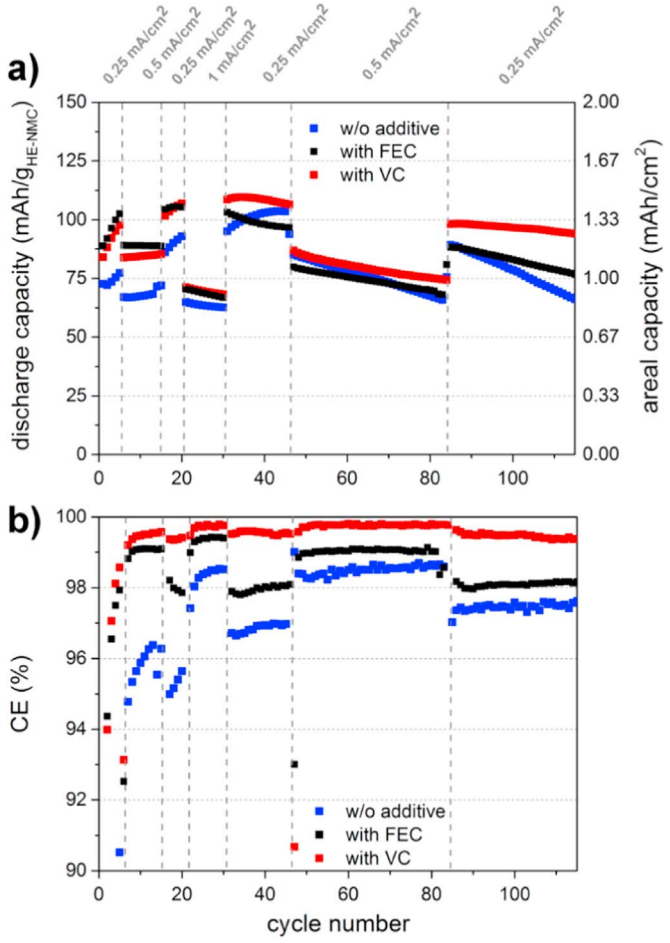

Fig. 6. Galvanostatic cycling of the full-cells between 1.8–4.6 V at different current density in dependence of VC and FEC addition. (w/o additive the cell was cycled between 1.8–4.5 V for the first 10 cycles).

3.4. Post–mortem investigations

To understand the structural differences of silicon anodes cycled in FEC- and VC-containing electrolytes, Swagelok half-cells (*versus* lithium metal) were disassembled after 300 cycles at 500 mA/g and were characterized by SEM/EDXS and XRD. Many excellent studies have already determined the chemical surface species of the SEI on silicon/carbon structures in dependence of FEC and VC additions, typically by XPS and FT-IR techniques [29,31,33,34]. With the use of SEM/EDXS and XRD we obtain further information about nanocrystalline phases and the structures on the electrode for different electrolyte compositions. Secondary electron (SE) images of the electrodes are shown in Fig. S5. No significant differences in the microstructure of the composites in dependence of the electrolyte composition are observed. Most important degradation phenomena likely occur on the nanoscale of the anode material, but a high-resolution transmission electron microscopic image would destroy any surface components with the electron beam [35]. However, SEM is useful to get information about the elemental concentration on each electrode by EDX spectroscopy (Table 3).

In the case of the sample cycled the additive-free electrolyte, fluorine and phosphorous are observed as traces, whereas the concentrations of carbon and oxygen describe the main components. A C/O ratio of 0.8 suggests a high decomposition of EC/DMC to form typical SEI compounds such as CH_3OCO_2Li, $(CH_2OCO_2Li)_n$ and Li_2CO_3 [53]. In contrast to this observation, the decomposition of the conductive salt $LiPF_6$ as only source for fluorine and phosphorous is therewith negligible. With the addition of FEC to the electrolyte the fluorine concentration remarkably increases without an increase of the phosphorous concentration. The C/O ratio is almost equal to 1. These results suggest a severely reduced decomposition of EC/DMC compared to the electrolyte without additive. For FEC a high decomposition rate has to be assumed to allow the formation of a relatively stable SEI what agrees well with current literature [35,37]. The electrode cycled in the presence of VC shows similar concentrations for F and P as the additive-free electrolyte. However, the silicon concentration and the C/O ratio is significantly higher (1.2), indicating a considerably lower EC/DMC decomposition due to the formation of a protective and flexible polymer film (presumably polycarbonate), as already proposed [33,34].

Table 3
Elemental composition of the nc-Si@C anode after 300 cycles determined by EDXS.

Sample	Si (at%)	C (at%)	O (at%)	F (at%)	P (at%)
w/o	5	41	52	2	u.[a]
FEC	5	35	37	22	u.[a]
VC	7	50	41	3	u.[a]

[a] Unverifiable.

Fig. 7a shows the EDX elemental mapping of an area of around 10 μm*6 μm for the FEC and VC additions. In both cases, carbon and silicon are well dispersed on the electrode material. However, fluorine is much finer dispersed and well distributed in the case of FEC addition, whereas for VC addition it is spread over the entire image with less fluctuation. This results indicates no particular deposition of fluorine and rather suggests traces of $LiPF_6$-related compounds. XRD was carried out in order to determine crystalline phases in the electrode structure. The patterns are shown in Fig. 7b. The crystalline structure of silicon disappeared because the silicon becomes amorphous during cycling [57]. The additive-free electrolyte exhibits no crystalline phases and the entire material is amorphous. With FEC we find nanocrystalline LiF (space group $Fm\bar{3}m$), which is likely embedded within the SEI [35]. The crystallite size of LiF is determined to 5 nm according to a Rietveld analysis, which is in good agreement with the finely dispersed fluorine in the elemental mapping (Fig. 7a). The pattern of the electrode cycled in VC again shows no reflections indicating no long range orders and observable crystalline phases.

4. Discussion

It is supposed that VC and FEC form similar polymeric structures [29,31,32,36]. In general, it is well accepted that the VC-derived SEI mainly consists of polycarbonates [33,34]. These polycarbonates may also be formed by the decomposition of FEC although there is still dispute on how the decomposition proceeds. Etacheri *et al.* proposed a defluorination of FEC to VC and HF resulting in polycarbonates and LiF. Our previous results support this assumption [35]. Other groups propose a ring opening mechanism for the FEC decomposition at first leading to fluorinated polymers or LiF [36,37]. Both mechanisms can occur as DFT calculations have shown [32]. All studies commonly reported large quantities of LiF, but the role of LiF in the SEI is not yet clear. Our results show that the LiF nanocrystals derived from FEC enhance the Li^+ ion conductivity inside the SEI, but cause a lower reversibility than that obtained with VC due to a less stable and continuously growing SEI resulting in an increase of the charge transfer resistance, presumably describable as electron transfer between silicon and carbon. In contrast, VC forms a dense and very flexible polycarbonate layer, which resists the dramatic volume changes of silicon without any fracture, thus preventing any electrolyte decomposition and further growth of the SEI. The VC-derived polycarbonate layer provides only low Li^+ ion conductivity due to the absence of any defects turning high rate performance tests to an almost impossible task. Using FEC instead of VC causes the precipitation of nanocrystalline LiF in the flexible polycarbonate layer. These LiF nanocrystals may

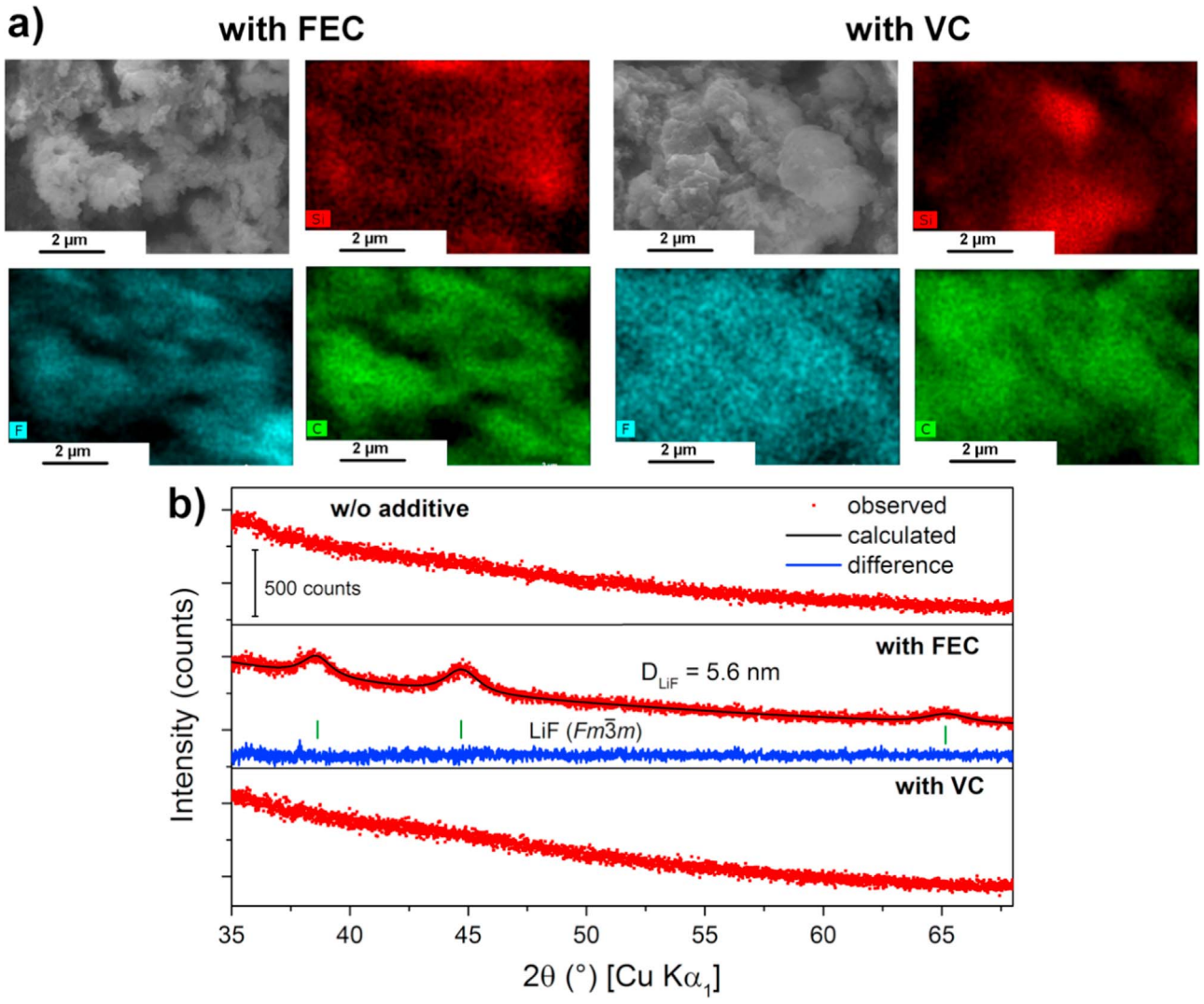

Fig. 7. a) EDXS elemental mapping of the cycled Si@C electrodes (for 300 cycles) in dependence of FEC or VC addition corresponding to the area shown in the SE image. The elements Si, F and C were recorded. b) XRD patterns of the cycled electrodes in dependence of the electrolyte compositions. A Rietveld analysis was performed with the structure model of LiF (space group Fm$\bar{3}$m) for the sample cycled in the FEC-based electrolyte.

cause defects in the dense and flexible layer allowing enhanced Li^+ ion conductivity and thus high rate capabilities. However, the FEC-derived polycarbonate SEI is less flexible and cannot resist the dramatic volume changes of silicon. Cracks and continuous electrolyte decomposition, preferentially of FEC, promote a slowly growing SEI, rich in LiF nanocrystals. Since LiF is certainly nonconductive for electrons like in principal most salts, the active silicon particle eventually loses electrical contact to the carbon scaffold resulting in a continuous capacity drop. We propose that the FEC- and VC-derived SEIs contain similar polymeric layers but modified with LiF nanocrystals in the case of FEC. Such enhanced ion conductivity by LiF deposition was also found by other groups [58,39,59]. However, it is unclear whether the enhanced Li^+ migration properties result from the LiF nanocrystals or defects formed at the interface of polymer and LiF. Compared to other SEI compounds such as semi organic lithium carbonates, LiOH or Li_2CO_3, the diffusion of Li^+ in LiF is rather low [60,61]. LiF is certainly a stable compound, but exhibits no flexibility and is a compact, inorganic substance, which therefore turns out to be rather disadvantageously on the reversibility of anode materials with large volume changes such as silicon. Altogether, the degradation mechanisms of silicon nanoparticles attached to a porous carbon scaffold are summarized as follows:

a) *Without additive,* two major degradation mechanisms occur in our silicon/carbon anode both attributed to the rapidly and continuously growing SEI:

I) Loss of electrical contact of individual silicon particles to the carbon scaffold.
II) Loss of ionic contact due to high film resistance suppressing Li^+ migration.

b) *With FEC* addition, the film resistance decreases dramatically and the SEI growth rate is considerably lower. However, the growth of the SEI cannot be completely suppressed and eventually a thick SEI is formed, causing a loss of electrical contact between individual silicon particles.

c) *With VC* addition, the growth of the SEI is nearly completely suppressed. The loss of electrical and ionic contact is prevented. However, the dense surface film causes only low Li^+ conductivity hindering the use of high current rates or thick electrode layers.

5. Conclusions

The VC-Additive for nano-silicon anodes clearly outperforms the additive FEC in terms of lifetime and efficiency owing to the formation of a very flexible surface film which survives the large volume changes

of silicon without surficial crack propagation. However, the surface film shows high film resistance for Li^+ migration as rate determining step, likely due to the absence of defects in the film structure turning VC unfavorable for high power applications. In contrast, the FEC-derived SEI shows less flexibility and reversibility compared to VC, but offers remarkable conductivity for Li^+ ions, which are excellent requirements for high power applications. We propose that the polymeric properties of both, VC and FEC-derived SEIs are equal; both consist of polycarbonates. However, in the case of FEC additional LiF nanocrystals are embedded within the surface film. These crystallites may cause defects in the homogeneous structure of the SEI allowing enhanced Li^+ ion conductivity, but at the expense of reversibility and cycle life. The inorganic and compact nanocrystals decrease the flexibility of the surface film resulting in cracks during the volume changes of the silicon particles, which eventually results in a loss of electrical contact to the carbon. In the absence of any electrolyte additive, both loss of electrical and ionic contact are responsible for fast degradation. We highlight the development of a facile and low-cost synthesis strategy for a high-capacitive nanostructured silicon anode for LIBs. Highly reversible areal capacities of around 5 mA h/cm^2 were demonstrated and our findings were successfully confirmed in real Li-ion systems with high-energy cathode materials. We believe that this study unveils the role of fluorine in FEC not only for silicon anodes, but likely for several other types of alloying anodes. Our findings open new strategies to develop advanced electrolyte additives for anode material with large volume changes during metalation or demetalation.

Acknowledgment

The authors thank Dr. Silke Hampel and Alexander Schubert for their valuable technical support and Cornelia Geringswald for thermogravimetric analysis. Steffi Kaschube is thanked for XPS measurements. We gratefully acknowledge the financial support from the German Federal Ministry of Education and Research (BMBF) through the Excellent Battery – WING center “Batteries - Mobility in Saxony” (Grant Nos. 03X4637B and 03X4637C).

Appendix A. Supporting information

Supplementary data associated with this article can be found in the online version at doi:10.1016/j.ensm.2016.08.002.

References

[1] N. Liu, Z. Lu, J. Zhao, M.T. McDowell, H.-W. Lee, W. Zhao, Y. Cui, Nat. Nanotechnol. 9 (2014) 187–192.
[2] D. Larcher, J.-M. Tarascon, Nat. Chem. 7 (2015) 19–29.
[3] Shmuel De-Leon Energy Ltd. Weekly Newsletter, vol. 319, 2016.
[4] N. Liu, H. Wu, M.T. McDowell, Y. Yao, C. Wang, Y. Cui, Nano Lett. 12 (2012) 3315–3321.
[5] C.K. Chan, H. Peng, G. Liu, Kevin McIlwartah, X.F. Zhang, R.A. Huggins, Y. Cui, Nat. Nanotechnol. 3 (2008) 31–35.
[6] H. Wua, Y. Cui, Nano Today 7 (2012) 414–429.
[7] W. Si, X. Sun, X. Liu, L. Xi, Y. Jia, C. Yan, O.G. Schmidt, J. Power Sources 267 (2014) 629–634.
[8] A. Magasinski, P. Dixon, B. Hertzberg, A. Kvit, J. Ayala, G. Yushin, Nat. Mater. 9 (2010) 353–358.
[9] T. Jaumann, M. Herklotz, M. Klose, K. Pinkert, S. Oswald, J. Eckert, L. Giebeler, Chem. Mater. 27 (2015) 37–43.
[10] K. Xu, Chem. Rev. 114 (2014) 11503–11618.
[11] H. Wu, G. C, J.W. Choi, I. Ryu, Y. Yao, M.T. McDowell, S.W. Lee, A. Jackson, Y. Yang, L. Hu, Y. Cui, Nat. Nanotechnol. 7 (2012) 310–315.
[12] M. Gauthier, D. Mazouzi, D. Reyter, B. Lestriez, P. Moreau, D. Guyomard, L. Roué, Energy Environ. Sci. 6 (2013) 2145.
[13] Y.-M. Lin, K.C. Klavetter, P.R. Abel, N.C. Davy, J.L. Snider, A. Heller, C.B. Mullins, Chem. Commun. 48 (2012) 7268–7270.
[14] B. Philippe, R. Dedryvère, M. Gorgoi, H. Rensmo, D. Gonbeau, K. Edström, J. Am. Chem. Soc. 135 (2013) 9829–9842.
[15] N.-S. Choi, K.H. Yew, K.Y. Lee, M. Sung, H. Kim, S.-S. Kim, J. Power Sources 161 (2006) 1254–1259.
[16] S. Sim, P. Oh, S. Park, J. Cho, Adv. Mater. 25 (2013) 4498–4503.
[17] Y. Hwa, W.-S. Kim, B.-C. Yu, S.-H. Hong, H.-J. Sohn, J. Phys. Chem. C 117 (2013) 7013–7017.
[18] Y. Hwa, W.-S. Kim, B.-C. Yu, H.-S. Kim, S.-H. Hong, H.-J. Sohn, J. Mater. Chem. A 1 (2013) 3733.
[19] E. Peled, F. Patolsky, D. Golodnitsky, K. Freedman, G. Davidi, D. Schneier, Nano Lett. 15 (2015) 3907–3916.
[20] C. Wang, H. Wu, Z. Chen, M.T. McDowell, Y. Cui, Z. Bao, Nat. Chem. 5 (2013) 1042.
[21] D. Mazouzi, N. Delpuech, Y. Oumellal, M. Gauthier, M. Cerbelaud, J. Gaubicher, N. Dupré, P. Moreau, D. Guyomard, L. Roué, B. Lestriez, J. Power Sources 220 (2012) 180–184.
[22] N. Delpuech, N. Dupré, D. Mazouzi, J. Gaubicher, P. Moreau, J.S. Bridel, D. Guyomard, B. Lestriez, Electrochem. Commun. 33 (2013) 72–75.
[23] B. Simon, J.-P. Boeuve, Rechargeable Lithium Electrochemical Cell, Patent No. US5626981, 1997.
[24] J.C. Burns, R. Petibon, K.J. Nelson, N.N. Sinha, Adil Kassam, B.M. Way, J.R. Dahn, J. Electrochem. Soc. 160 (2013) A1668–A1674.
[25] H. Wu, G. Yu, L. Pan, N. Liu, M.T. McDowell, Z. Bao, Y. Cui, Nat. Commun. 4 (2013) 1–6.
[26] L. Chen, K. Wang, X. Xie, J. Xie, Electrochem. Solid-State Lett. 9 (2006) A512–A515.
[27] M. Nie, J. Demeaux, B.T. Young, D.R. Heskett, Y. Chen, A. Bose, J.C. Woicik, B.L. Lucht, J. Electrochem. Soc. 162 (2015) A7008–A7014.
[28] L. Leveau, B. Laik, J.-P. Pereira-Ramos, A. Gohier, P. Tran-Van, C.-S. Cojocaru, Electrochim. Acta 157 (2015) 218–224.
[29] S. Dalavi, P. Guduru, B.L. Lucht, J. Electrochem. Soc. 159 (2012) A642–A646.
[30] S. Uchida, M. Yamagata, M. Ishikawa, J. Electrochem. Soc. 162 (2015) A406–A412.
[31] V. Etacheri, O. Haik, Y. Goffer, G.A. Roberts, I.C. Stefan, R. Fasching, D. Aurbach, Langmuir 28 (2012) 965–976.
[32] J.M. Martinez de la Hoz, P.B. Balbuena, Phys. Chem. Chem. Phys. 16 (2014) 17091–17098.
[33] D. Aurbach, K. Gamolsky, B. Markovsky, Y. Gofer, M. Schmidt, U. Heider, Electrochim. Acta 47 (2002) 1423–1439.
[34] L.E. Ouatani, R. Dedryvère, C. Siret, P. Biensan, S. Reynaud, P. Iratçabal, D. Gonbeau, J. Electrochem. Soc. 156 (2009) A103–A113.
[35] T. Jaumann, J. Balach, M. Klose, S. Oswald, U. Langklotz, A. Michaelis, J. Eckert, L. Giebeler, Phys. Chem. Chem. Phys. 17 (2015) 38.
[36] X. Chen, X. Li, D. Mei, J. Feng, M.Y. Hu, J. Hu, M. Engelhard, J. Zheng, W. Xu, J. Xiao, J. Liu, J.-G. Zhang, ChemSusChem 7 (2014) 549–554.
[37] C. Xu, F. Lindgren, B. Philippe, M. Gorgoi, F. Björefors, K. Edström, T. Gustafsson, Chem. Mater. 27 (2015) 2591–2599.
[38] Q. Zhang, X. Xiao, W. Zhou, Y.-T. Cheng, M.W. Verbrugge, Adv. Energy Mater. 5 (2015) 1401398.
[39] K. Schroder, J. Alvarado, T.A. Yersak, J. Li, N. Dudney, L.J. Webb, Y.S. Meng, K.J. Stevenson, Chem. Mater. 27 (2015) 5531–5542.
[40] Z. Chen, K. Amine, J. Electrochem. Soc. 153 (2006) A1221–A1225.
[41] T. Jaumann, J. Balach, M. Klose, S. Oswald, J. Eckert, L. Giebeler, J. Electrochem. Soc. 163 (2016) A557–A564.
[42] H. Shin, J. Park, A.M. Sastry, W. Lu, J. Electrochem. Soc. 162 (2015) A1683–A1692.
[43] Y. Li, F. Lian, L. Ma, C. Liu, L. Yang, X. Sun, K. Chou, Electrochim. Acta 168 (2015) 261–270.
[44] E. Markevich, G. Salitra, K. Fridman, R. Sharabi, G. Gershinsky, A. Garsuch, G. Semrau, M.A. Schmidt, D. Aurbach, Langmuir 30 (2014) 7414–7424.
[45] J.C. Burns, A. Kassam, N.N. Sinha, L.E. Downie, L. Solnickova, B.M. Way, J.R. Dahn, J. Electrochem. Soc. 160 (2013) A1451–A1456.
[46] L. Ma, J. Xia, X. Xia, J.R. Dahn, J. Electrochem. Soc. 161 (2014) A1495–A1498.
[47] Hui Wu, Y. Cui, Nano Today 7 (2012) 414–429.
[48] E.J. Henderson, J.A. Kelly, J.G.C. Veinot, Chem. Mater. 21 (2009) 5426–5434.
[49] L. Lutterotti, D. Chateigner, S. Ferrari, J. Ricote, Thin Solid Films 450 (2004) 34–41.
[50] C.M. Hessel, E.J. Henderson, J.G.C. Veinot, Chem. Mater. 18 (2006) 6139–6146.
[51] A.M. Wilson, J.R. Dahn, J. Electrochem. Soc. 142 (1995) 326–332.
[52] H. Kim, M. Seo, M.-H. Park, J. Cho, Angew. Chem. Int. Ed. 49 (2010) 2146–2149.
[53] D. Aurbach, B. Markovsky, I. Weissman, E. Levi, Y. Ein-Eli, Electrochim. Acta 45 (1999) 67–86.
[54] J.P. Schmidt, T. Chrobak, M. Ender, J. Illig, D. Klotz, E. Ivers-Tiffée, J. Power Sources 196 (2011) 5342–5348.
[55] D. Aurbach, J. Power Sources 89 (2000) 206–218.
[56] J. Guo, A. Sun, X. Chen, C. Wang, A. Manivannan, Electrochim. Acta 56 (2011) 3981–3987.
[57] J. Li, J.R. Dahn, J. Electrochem. Soc. 154 (2007) A156–A161.
[58] S. Choudhury, L.A. Archer, Adv. Electron. Mater. 2 (2016) 1500246.
[59] R. Jorn, R. Kumar, D.P. Abraham, G.A. Voth, J. Phys. Chem. C 117 (2013) 3747–3761.
[60] K. Tasaki, A. Goldberg, J.-J. Lian, M. Walker, A. Timmons, S.J. Harris, J. Electrochem. Soc. 156 (2009) A1019–A1027.
[61] H. Yildirim, A. Kinaci, M.K.Y. Chan, J.P. Greeley, ACS Appl. Mater. Interf. 7 (2015) 18985–18996.